Image Segmentation Using Multiresolution Fourier Transform

Chang-Tsun Li, Roland Wilson
Department of Computer Science,
University of Warwick,
Coventry

September 18, 1995

Abstract

In this report, the Multiresolution Fourier Transform (MFT) is utilised as an approach to the segmentation of images based on the analysis of local properties in the spatial frequency domain. Six major steps are adopted to implement the segmentation of images in this work. Firstly, The Laplacian Pyramid method is used as the filter to create the high-pass filtered image. Secondly, Multiresolution Fourier Transform (MFT) is applied to transform the high-pass filtered image into a double-sized 'spectrum image' consisting of local spectra. Thirdly, a pair of representative centroid vectors are estimated as description of the local spectrum. Subsequently, the variances are utilised as a criterion to determine if the block of the image contains one or multiple features. A priori knowledge of the starting scale is not required. If a local region of the image at a lower resolution level is estimated to be containing multiple features, the algorithm goes to a higher resolution level and re-does the analysis until a single feature is found in the sub-block or a specific level is reached. If a block containing single feature is identified, the next step is taken to extract the orientation and position of the feature in the block. Finally, the accuracy of the estimated position of the centroid of the local feature is checked.

Contents

List of Figures

1 Introduction

Traditionally, image segmentation has been approached either from localisation in position using edge or boundary information, or from localisation in class space using regional information.

1.1 Segmentation based on regional information

Features of textured images can be segmented based on regional information such as coarseness and fineness, regularity and orientation. The simplest approach to segmentation is thresholding the grey level image by using the histogram of the image as the class space. The histogram contains only global information, but retains no positional information. Therefore uncertainty about position becomes inevitable. Some more sophisticated methods have been adopted to overcome this draw back. Depending on the type of textures, these methods are divided into structural and statistical approaches [6]. Structural approaches such as autocorrelation consider a textured image as composed of repeating or periodical texture elements like tile wall. Statistical approaches such as co-occurrence matrices, auto-regression, maximum entropy power spectrum estimation and Relaxation Labelling [11] consider the texture as a set of statistics extracted from local image measurements. Generally, they are good for textures with random spatial arrangements.

1.2 Segmentation based on positional information

This class of approaches involves the detection of luminance discontinuities such as lines, edges and boundaries in small neighbourhood. To find out their orientation and position, local operations such as convolving a kernel operator/windowing function with the image are used. However, noise or random fluctuation also reflect discontinuities which are very likely to be detected along with the features of interest. Some approaches such as gradient methods, spatial averaging, frequency domain methods and zero crossing have been attempted to achieve noise immunity. Unfortunately most of them are still limited by some degree of uncertainty, i.e. to achieve better noise immunity, averaging over a larger region is necessary. But increasing the averaging region size loses the positional resolution in return.

1.3 Uncertainty

The main difficulty in image segmentation is that classification of class space requires global information, which reduces the certainty of 'where' the position of the edges or boundaries are [15]. Similarly, edges or boundaries can be detected by analysing small neighbourhood, which reduces the certainty about 'what' class this is. Recently, attempts have been made to incorporate both regional and positional information. Unfortunately, simultaneous localisation in both space class and position is always a dilemma. Higher certainty in one aspect tends to be obtained at the expense of the other. Multiresolution methods such as the Wavelet Transform (WT) and Multiresolution Fourier Transform (MFT) [3] [14] are therefore used to allow a trade-off between resolution in class space and position.

Among the multiresolution methods, MFT enables the analysis to be carried out over a range of different levels with kernels/windowing functions of various size. By varying the resolution in both spatial and spatial frequency domains, the uncertainty is confined to a reasonable extent while the computation efficiency still maintained. Detailed description of MFT is given in Section 2.

2 Multiresolution Fourier Transform

MFT is a combination of Wavelet Transform (WT) and Short Time Fourier Transform (STFT) [14] which is able to perform local Fourier transformation over a range of scales. A MFT coefficient at level l is identified by three parameters: spatial co-ordinate $\vec{\xi}(l)$, frequency co-ordinate $\vec{\omega}(l)$ and scale $\gamma(l)$. A 2-D MFT coefficient can be represented by

$$\hat{f}(\vec{\xi}(l), \vec{\omega}(l), \gamma(l)) \ = \sum \ w_n(\vec{\xi}(l) - \vec{\xi'}(l)) \ f(\vec{\xi'}(l)) \ e^{[-j\vec{\xi'}(l)\vec{\omega}(l)]} \tag{1}$$

where $w_n(\vec{\xi}(l) - \vec{\xi'}(l))$ is a Finite Prolate Spheroidal Sequence (FPSS) acting as a windowing function with maximal energy concentration in both spatial and spatial frequency domain.Therefore each level of MFT resembles a Short Time Fourier Transform (STFT). $f(\vec{\xi'}(l))$ represents the original N $\times$ N image in the spatial domain. Figure 1 shows the general structure of the MFT. At the lowest level (level 0), a single block covers the whole original image in spatial domain, therefore MFT is actually the DFT of the original image at this level. While at the highest level, each of the N $\times$ N blocks covers only one point in spatial domain, so the MFT is just the original image itself. The other levels in between are STFTs with windowing functions of different size.

MFT has following merits which are important to image analysis [3] [7]:
(i)Space Linearity: MFT is a hierarchical structure of STFT's, and because STFT is linear, therefore MFT inherits the linear property. Ensuring linearity, the response of the filtering operation on the signal and addition can be predicted.
(ii)Locality: each level of MFT performs local operation in each domain. This locality property enables the differentiation between texture fields because there is evidence that texture discrimination is achieved in relatively small neighbourhood [8].
(iii)Invertibility: Since STFT is invertible, the MFT has the similar property. This

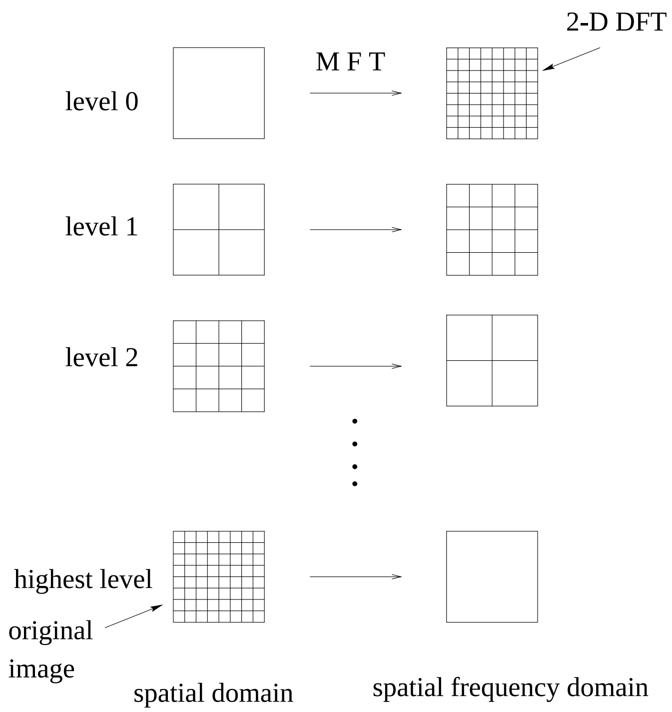

Figure 1: Structure of 2-D MFT at different levels

property minimises errors due to the information loss during the transformation from one domain to another.

3 Image Segmentation

Six major steps are adopted to implement the segmentation of images in this work. Firstly, The Laplacian Pyramid method [2] is used as the filter to create the high-pass filtered image. Secondly, Multiresolution Fourier Transform (MFT) is applied to transform the high-pass filtered image into a double-sized spectrum image consisting of local spectra. Thirdly, a pair of representative centroid vectors is estimated as description of the local spectrum. Subsequently, the variances are utilised as a criterion to determine if the block of the image contains one or multiple features. A priori knowledge of the starting scale is not required. If a local region of the image at a lower resolution scale is estimated to be containing multiple features, the algorithm goes to a higher resolution level and re-does the analysis until a single feature is found in the subregion or the specific level is reached. If a block containing single feature is identified, the next step is taken to extract the orientation and position of the feature in the block. Finally, the accuracy of the estimated position of the centroid of the feature is checked.

3.1 Laplacian Pyramid

Laplacian Pyramid method [2] uses a unimodal Gaussian-like weighting function/kernel operator to convolve with the image. The result of this local operation on each pixel is a low-pass filtered version of the original image. A high-pass filtered image is then obtained by subtracting the low-pass filtered image from the original image.

Given $g_0(x, y)$ as the original image, sub-sampling process can be applied to create a Gaussian Pyramid with $g_0(x, y)$ as the bottom level and $g_l(x, y)$, low-pass filtered version, on the top of $g_{l-1}(x, y)$. For $0 < l \leq N$,

$$g_l(x, y) = \sum_{m=0}^{3} \sum_{n=0}^{3} w(m, n)\, g_{l-1}(2x + m, 2y + n) \tag{2}$$

N + 1 is the number of levels in the Gaussian Pyramid. Since the sampling density are decreased by a factor of 2, the size of the 2-D image $g_l(x, y)$ is a quarter of $g_{l-1}(x, y)$.

Laplacian Pyramid is a sequence of difference images $L_0(x, y)$, $L_1(x, y)$, $L_2(x, y)$, $\cdots$, $L_{N-1}(x, y)$. Each is the difference image between two levels of the Gaussian Pyramid. To obtain $L_l(x, y)$, The $g_{l+1}(x, y)$ in the Gaussian Pyramid must be expanded to the same size as $g_l(x, y)$. Thus for $0 \leq l < N$, the expanded version of $g_{l+1}(x, y)$ is

$$g_l'(x, y) \;=\; 4 \sum_{m=0}^{3} \sum_{n=0}^{3} w(m, n)\, g_{l+1}(\frac{x + m}{2}, \frac{y + n}{2}) \tag{3}$$

and the difference images/high-pass filtered images are

$$L_l(x, y) \;=\; g_l(x, y) \;-\; g_l'(x, y) \tag{4}$$

Since only the four terms for which $\frac{x+m}{2}$ and $\frac{y+n}{2}$ are integers are included in equation (3), the sum is multiplied by 4 to reflect the fact that there are 16 pixels covered by the weighting function.

It can be proved that the original image $g_0(x, y)$ can be recovered by expanding L_{N-1} once and add it to L_{N-2}, then expand this image sum once and add it to L_{N-3}, and so on until level 0 is reached. In this work, L_0 is taken as the high-pass filtered version of the original image. Figure 2 shows the process of establishing a Laplacian Pyramid. Figure 3 is a testing image and its high-pass filtered version, $L_0(x, y)$.

3.2 Application of Multiresolution Fourier Transform

Once the high-pass filtered image with size $N \times N$ is obtained, MFT is applied to transformed it into a $2\,N \times 2\,N$ spectral image in spatial frequency domain. Figure 4 shows the MFT spectra of Figures 3(b) at level 4. The grids are added for easy reference and the arrows are added to serve some purpose which is discussed latter.

The local spectra of the MFT are obtained by discrete DFT. The 'wrap-around' artifacts therefore exist in some blocks, especially the ones in which linear features are

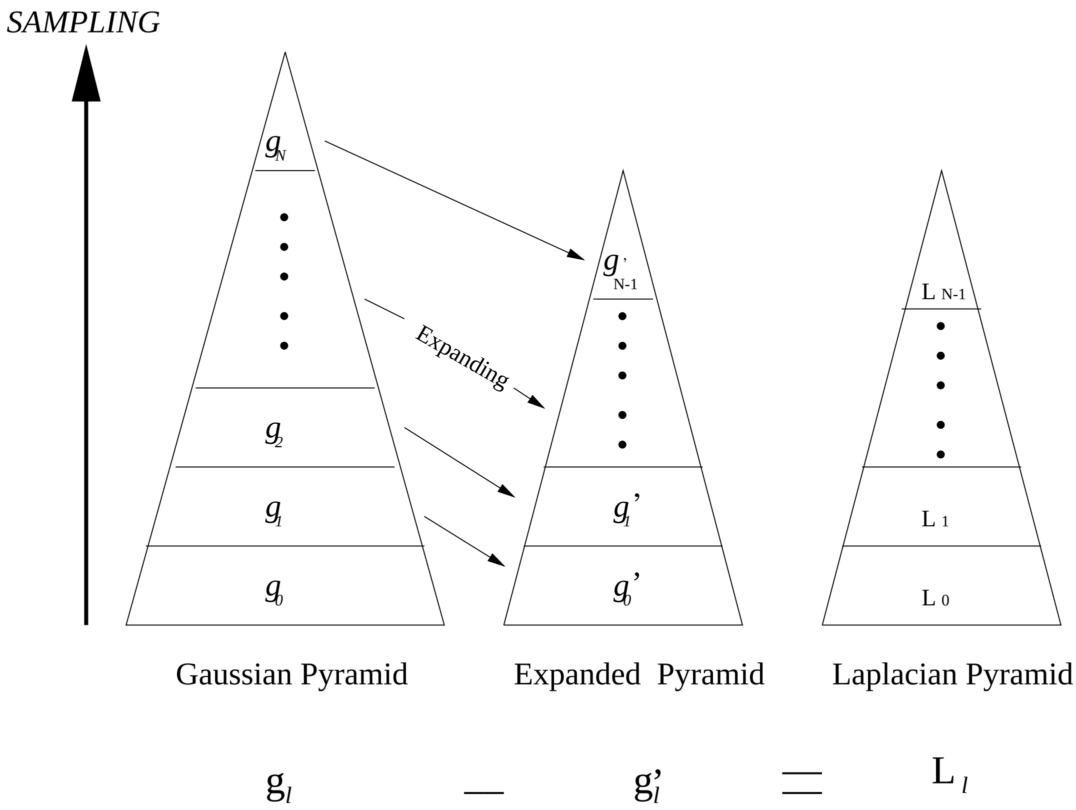

Figure 2: From Gaussian Pyramid to Laplacian Pyramid

present and the spectral energy does not decrease significantly at higher frequencies along the main axis of the energy ellipse [9]. Figure 5 shows the local spectrum with artifact of a linear feature. In this work, artifacts are not predicted and not tackled, and this affects the accuracy of orientation estimation.

3.3 Estimation of centroid vectors

Hsu has used a pair of centroid vectors to represent a local spectrum for texture analysis and synthesis [7]. Fourier spectrum is used to implement his algorithm. Similar approach is used in this work. But after some experiment, power spectrum , in stead of Fourier spectrum, is used to implement the following algorithm in this work in order to get more accurate feature orientation. Details about the estimation of feature orientation will be given later. To find the centroid vector pair, $\hat{f}(\vec{\omega}_{x,y})$, the values of two variable angles θ_1 and θ_2 are to be determined such that

$$V_s = \frac{M_1(\theta_1, \theta_2)\ \sigma_1^2(\theta_1, \theta_2) + M_2(\theta_1, \theta_2)\ \sigma_2^2(\theta_1, \theta_2)}{M_1(\theta_1, \theta_2)\ +\ M_2(\theta_1, \theta_2)} \tag{5}$$

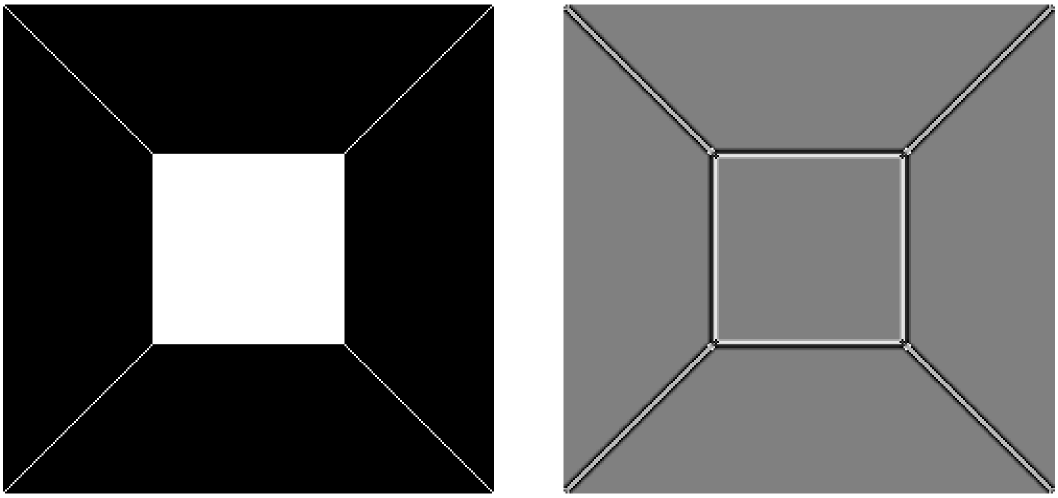

(a) Original test image (size: 256 X 256)　　(b) High-pass filtered version of (a)

Figure 3: A testing image and its high-pass filtered version

is minimum, where

$$M_i(\theta_1, \theta_2) = \sum_{\vec{\omega} \in \Lambda_i(\theta_1, \theta_2)} |\hat{f}(\vec{\omega})|^2 \qquad i = 1, 2 \tag{6}$$

$$\sigma_i^2(\theta_1, \theta_2) = \frac{1}{M_i(\theta_1, \theta_2)} \sum_{\vec{\omega} \in \Lambda_i(\theta_1, \theta_2)} |\hat{f}(\vec{\omega})|^2 \, \|\vec{\omega} - \vec{\mu}_i(\theta_1, \theta_2)\|^2 \qquad i = 1, 2 \tag{7}$$

$\mu_i(\theta_1, \theta_2)$ is the centroid vector

$$\mu_i(\theta_1, \theta_2) = \frac{1}{M_i(\theta_1, \theta_2)} \sum_{\vec{\omega} \in \Lambda_i(\theta_1, \theta_2)} |\hat{f}(\vec{\omega})|^2 \, \vec{\omega} \qquad i = 1, 2 \tag{8}$$

and $\Lambda_1(\theta_1, \theta_2)$ and $\Lambda_2(\theta_1, \theta_2)$ are the sets of coordinates in each of the two segments of the half-plane starting at angle θ_1 and divided at angle θ_2. To find the minimum V_s, each different combination of angles θ_1 and θ_2 is tested. The intervals of θ_1 and θ_2 are $0 \leq \theta_1 < \pi$ and $\theta_1 < \theta_2 < \theta_1 + \pi$. Taking advantage of the Hermitian symmetry of the Fourier transform, only a half plane of the local spectrum/region need to be analysed.

In Figure 6 , θ_1 is used to divide the local spectrum into two half-planes and θ_2 is used to sub-divide the half-plane starting at θ_1 into two segments, Λ_1 and Λ_2.

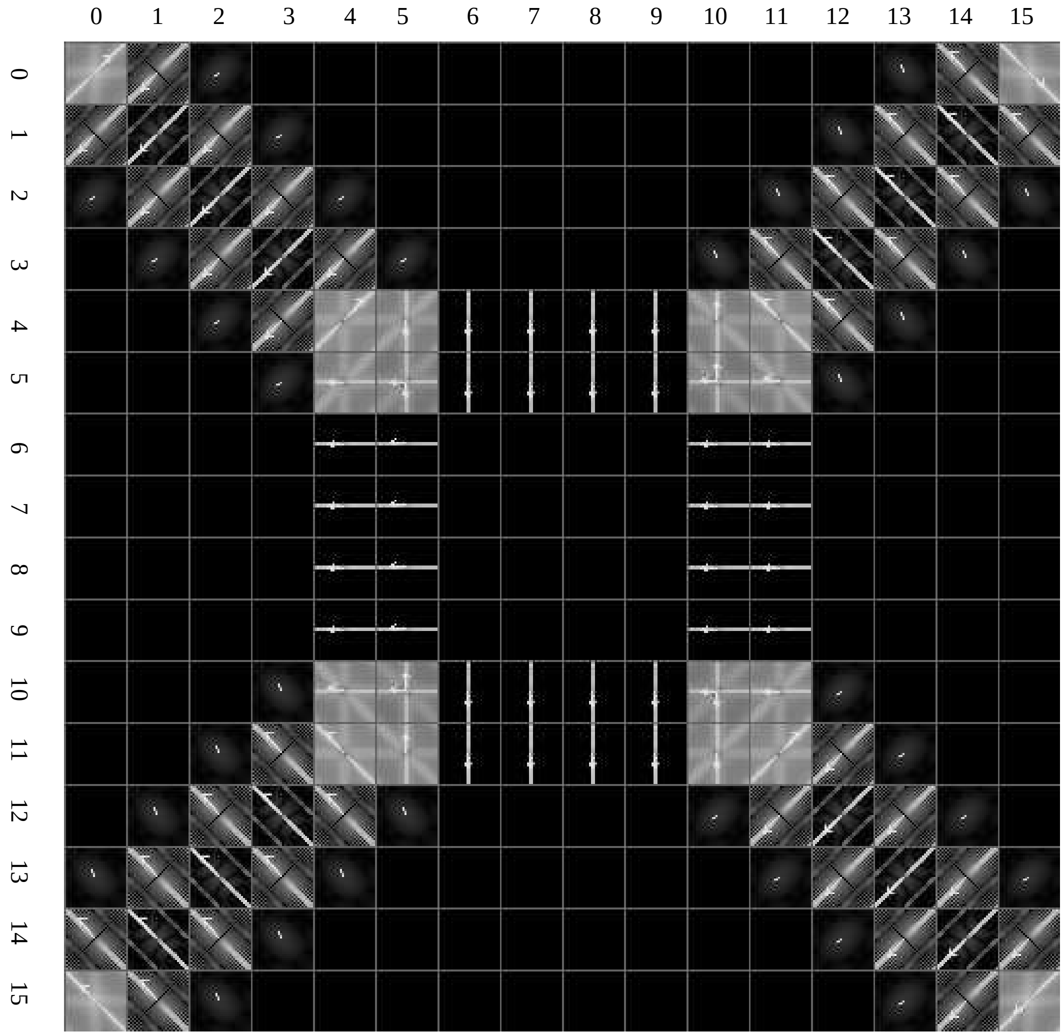

Figure 4: MFT spectra of Figures 3(b) at level 4

3.4 Minimum variance ratio criterion

After V_s, θ_1 and θ_2 in equation (5) are found, the centroid vector, $\vec{\mu}_h(\theta_1)$, of the half-plane starting at θ_1 is estimated in order to calculate the variance, V_h, of the half-plane.

$$V_h = \frac{1}{M_h(\theta_1)} \sum_{\vec{\omega}\in\Lambda(\theta_1)} |\hat{f}(\vec{\omega})|^2 \, \|\vec{\omega} - \vec{\mu}_h(\theta_1)\|^2 \tag{9}$$

$$M_h(\theta_1) \;=\; \sum_{\vec{\omega}\in\Lambda(\theta_1)} |\hat{f}(\vec{\omega})|^2 \tag{10}$$

$\vec{\mu}_h(\theta_1)$ is the centroid vector of the half-plane

$$\vec{\mu}_h(\theta_1) \;=\; \frac{1}{M_h(\theta_1)} \sum_{\vec{\omega}\in\Lambda(\theta_1)} |\hat{f}(\vec{\omega})|^2 \, \vec{\omega} \tag{11}$$

and $\Lambda(\theta_1)$ is the set of coordinates of the half-plane starting at angle θ_1. Figure 4 shows the MFT spectrum of Figures 3(b) at level 4. Single-a arrows are added to represent the half-plane centroid vector, $\vec{\mu}_h(\theta_1)$, of the block and double-arrows are added to represent each centroid vector, $\vec{\mu}_i(\theta_1, \theta_2)$ of the two segments of the block's half-plane.

Once V_h is found, the variance ratio $\frac{V_s}{V_h}$ is utilised to classify whether the local spectrum contains single or multiple features. Given a specific threshold α, if

$$\frac{V_s}{V_h} \;\geq\; \alpha \;, \qquad 0 \;<\; \alpha \;\leq 1 \tag{12}$$

then the block is classified as one containing only one feature, otherwise, it contains multiple features. If a block contains multiple features, it will be divided into 4 sub-blocks. Each of these will be re-estimated at the higher resolution level until a single feature is found or the specific level, where the block is too small to be analysed, is reached.

3.5 Locating the features

To locate a feature, both the feature's orientation and the centroid are to be calculated. Some researchers [3] [5] [13] have used 'inertia tensor' [1] to estimate feature orientation with satisfactory results. In this work, we estimate local feature orientation by calculating the argument of the centroid vector of the half-plane starting at angle θ_1 in equation (11). For the blocks containing single feature, the orientation of $\vec{\mu}_h(\theta_1)$ in equation (11) is the orientation of the axis along which the energy cluster. Therefore, $Arg[\vec{\mu}_h(\theta_1)]$ is taken as the feature's orientation in the spatial frequency domain. Since we are seeking the feature's orientation in the spatial domain, $\pi/2$ is added to reflect the fact that feature's orientation in spatial frequency domain and in spatial domain are perpendicular to each other.

As described in [3], [4], [10] and [12], positional informations are contained in the phase of the Fourier transform. The position of the centroid of a local feature can be estimated by averaging phase difference over all frequencies. Given the spectrum of a local linear feature as [4]

$$\hat{f}(u,v) = \begin{cases} |\hat{f}(u,v)| \, e^{-j(ux \,+\, vy \,+\, \varepsilon)} & \text{if } x\cos\theta + y\sin\theta > 0 \\ |\hat{f}(u,v)| \, e^{-j(ux \,+\, vy \,-\, \varepsilon)} & \text{otherwise} \end{cases} \tag{13}$$

where (x, y) is position of the centroid of the linear feature, ε is the phase constant and θ is the orientation of the feature in frequency domain. Since there is a phase jump of 2ε at frequencies along the line where $x\cos\theta + y\sin\theta = 0$, only the coefficients in the half-plane, the shaded area Θ_θ in Figure 7 , satisfying $x\cos\theta + y\sin\theta = 0$ are used to estimate the position of the centroid of the feature. The autocorrelations of the image spectrum in both u and v dimension respectively are

$$\rho_u = \frac{\sum_{u,v \in \Theta_\theta} \hat{f}(u,v)\,\hat{f}^*(u+u',v)}{\sum_{u,v \in \Theta_\theta} |\hat{f}(u,v)|^2} \tag{14}$$

$$\rho_v = \frac{\sum_{u,v \in \Theta_\theta} \hat{f}(u,v)\,\hat{f}^*(u,v+v')}{\sum_{u,v \in \Theta_\theta} |\hat{f}(u,v)|^2} \tag{15}$$

where u' and v' are sampling intervals in u and v dimensions respectively. By substituting equation (13) for both equations (14) and (15), the estimate of the centroid position (x,y) can be given as

$$x_0 = \frac{Arg(\rho_u)}{u'} \tag{16}$$

$$y_0 = \frac{Arg(\rho_v)}{v'} \tag{17}$$

Since the sampling intervals in this work are $\frac{2\pi}{N}$, therefore equations (16) and (17) become

$$x_0 = \frac{Arg(\rho_u)}{\frac{2\,\pi}{N}} \tag{18}$$

$$y_0 = \frac{Arg(\rho_v)}{\frac{2\,\pi}{N}} \tag{19}$$

3.6 Accuracy check

Once the position of the centroid of the feature has been estimated, The accuracy of the estimated position should be check. As used in [4], the synthesised local spectrum is obtained by replacing x and y in equation (13) with x_0 and y_0 respectively:

$$\tilde{f}(u,v) = |\hat{f}(u,v)|\; e^{-j(ux_0\,+\,vy_0)} \tag{20}$$

The accuracy parameter γ is then calculated by correlating the real local spectrum $\hat{f}(u,v)$ and its synthesised counterpart $\tilde{f}(u,v)$:

$$\gamma = \frac{\sum_{u,v \in \Theta_\theta} \hat{f}(u,v)\,\tilde{f}^*(u,v)}{\sum_{u,v \in \Theta_\theta} |\hat{f}(u,v)|^2} \tag{21}$$

From the above equation, it is easy to see that $\gamma = 1$ if the estimated centroid position (x_0, y_0) is exactly equal to the real centroid position (x, y). Otherwise, $\gamma < 1$. The closer to 1 γ is, the more accurate the estimated centroid position is. If γ is higher than a given threshold, all the estimated parameters of the current block are deemed accurate enough and no further estimation at higher level are needed. If γ is less than the given threshold, despite the fact that equation (12) is satisfied, all the estimated parameters are to be discarded and further estimation is needed at higher level.

4 Experiments

Choosing optimal values for the thresholds α and γ requires some experiments to be performed on different images. Figure 8(a) shows the experimental result of the test image in Figure 3 with $\alpha = 0.50$ and threshold value $\gamma = 0.0$. The features/edges of the original image are extracted at level 4, 5 and 6. The accuracy is satisfactory except at the four corners of the square where three features meet. Where the three features meet around the four corners of the square, the local spectrum disperses. This causes the tilting of the features in blocks (4,5), (5,4), (4,10), (5,11), (10,4), (11,5), (10,11) and (11,10) at level 4. In Figure 8(b), with the same threshold of $\alpha = 0.50$ but $\gamma = 0.90$, the γs estimated in the blocks around the corners of the square at level 4 are less than 0.90, so higher levels are reached and features found in finer blocks are as accurate as other features found at level 4. But very close to the vertices of the square where three features meet, the features are still not detected even at level 6 with block size 4×4 because of the spectral dispersion. The features in the blocks around the image corners are also not detected even at level 5 because the 'border extension effect' occurs in the building process of the Laplacian Pyramid.

Figure 9 shows the image 'Girl' and its high-pass filtered version. Figure 10 shows images of the features extracted from Figure 9 with $\alpha = 0.45$, $\gamma = 0.0$ and 0.70 respectively. Without checking the accuracy of estimated position of the centroid of the features by setting $\gamma = 0.0$, it is easy to see from Figure 10(a) that large edges of the image can be extracted with low threshold value of variance ratio $\alpha = 0.45$ without going to a higher level. However, edges detected at lower level (bigger blocks) do not reflect larger curvatures. To get a smoother segmentation result, a higher value of γ is needed. The smoothness is apparent in Figure 10(b) with $\gamma = 0.7$. Another way to get a smoother segmentation result with the same value of γ is to use higher value of α. Enhanced smoothness is also apparent in Figure 11 (a) with $\alpha = 0.55$ and $\gamma = 0.0$ although the result is not as good as Figure 10(b). Again the result can still be improved with higher value of γ. Figure 11(b) shows the result of 'Girl' with $\alpha = 0.55$ and $\gamma = 0.7$. Figure 12 (a) and (b) show the segmentation result of 'Girl' with $\alpha = 0.60$, $\gamma = 0.0$ and 0.70 respectively.

Figure 13 shows the experiment results on the image of a portion of a reptile skin, a typical structural textured image. Figure 13(a) is the original image while Figure 13(b) is the high-pass filtered version of the original image. Figure 13(c) shows the extracted features/edges of original image with $\alpha = 0.5$ and $\gamma = 0.0$. Figure 13(d) shows the segmentation result with $\alpha = 0.5$ again and $\gamma = 0.7$.

5 Conclusion and Further Work

With the merits of MFT, uncertainty between class space and position is confined to a reasonable degree. The flexibility of varying through different levels of MFT requires no a priori knowledge about the choice of starting level. This makes the algorithm versatile for segmenting images with edges/boundaries of different curvatures or crossing edges/boundaries.

Experiments have shown satisfactory results applying variance as decision criterion for detecting edges/boundaries. The next phase of this work is to make it a general framework capable of achieving segmentation of both textured and non-textured images.

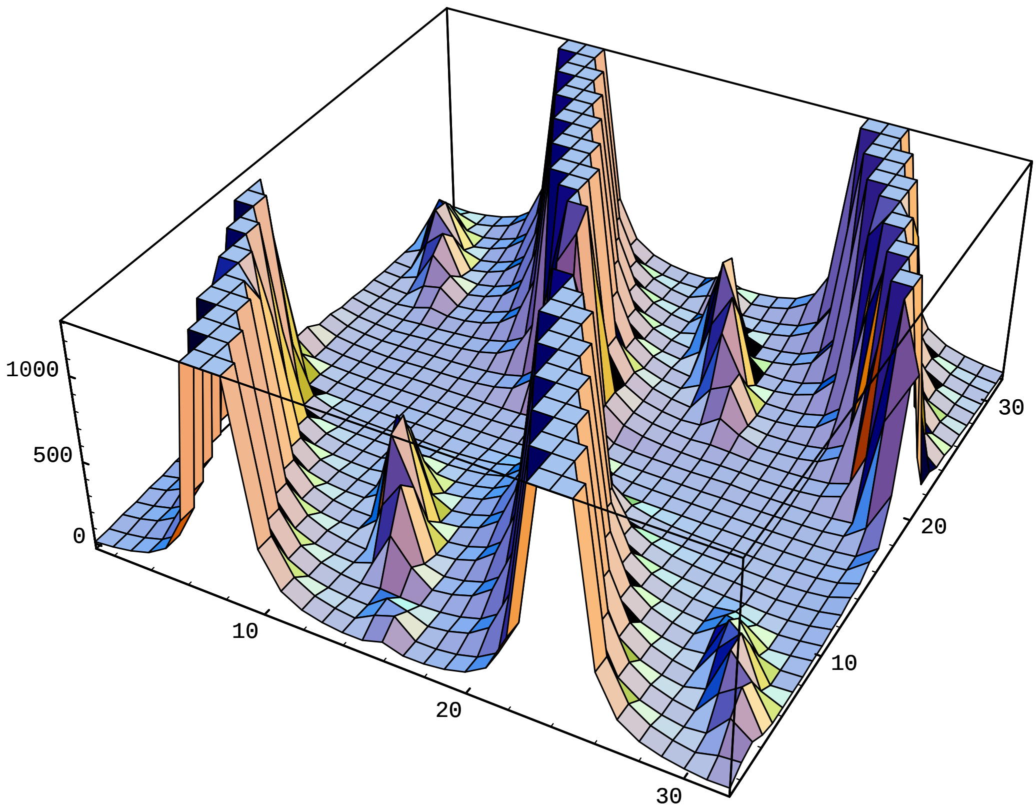

Figure 5: "Wrap-around" artifact in local spectrum

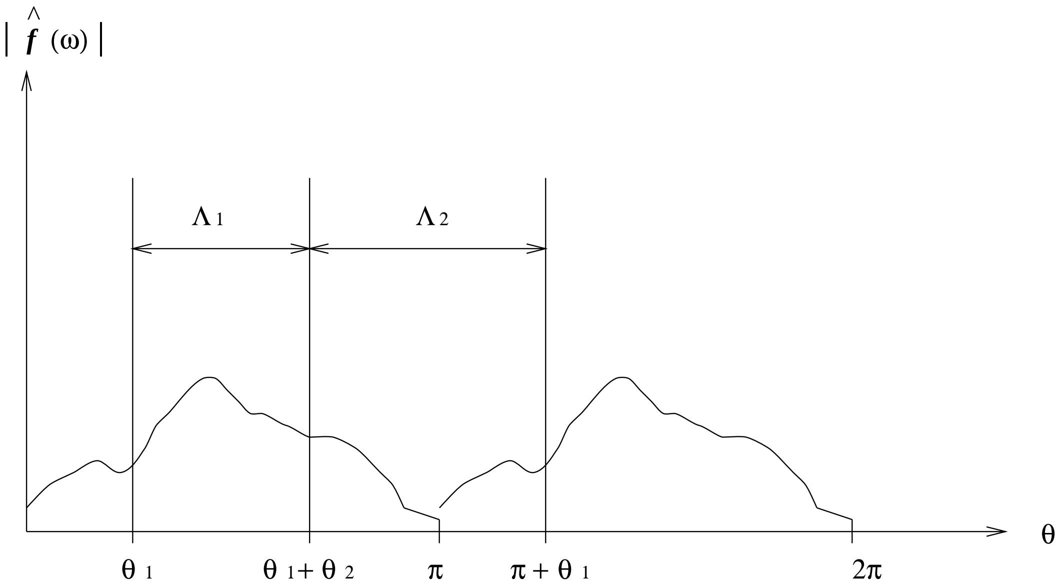

Figure 6: Division of a spectral half-plane into two segments by θ_1 and θ_2.

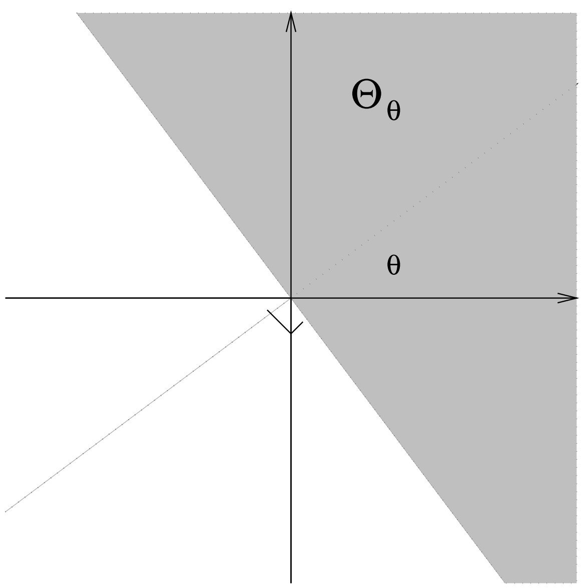

Figure 7: The shaded half-plane where $x \cos\theta + y \sin\theta > 0$

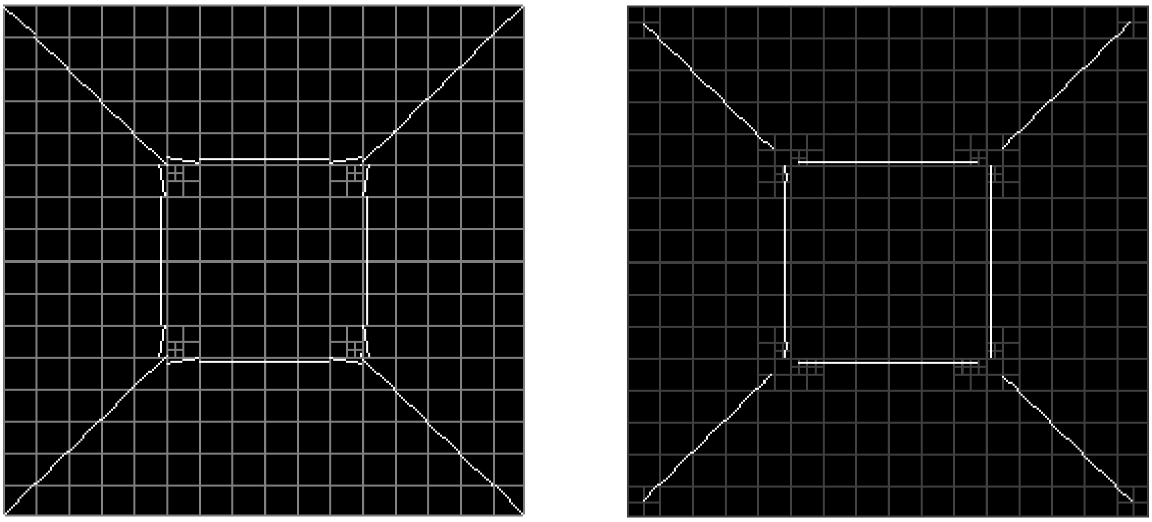

(a) $\alpha = 0.5, \gamma = 0.0$ (b) $\alpha = 0.5, \gamma = 0.9$

Figure 8: Segmentation result of the testing image in Figure 3 with $\alpha = 0.50$ and different value of γ at different levels

(a) Original image of "Girl" (Size 256 X 256) (b) High-pass filtered version of (a).

Figure 9: Image 'Girl' and its high-pass filtered version

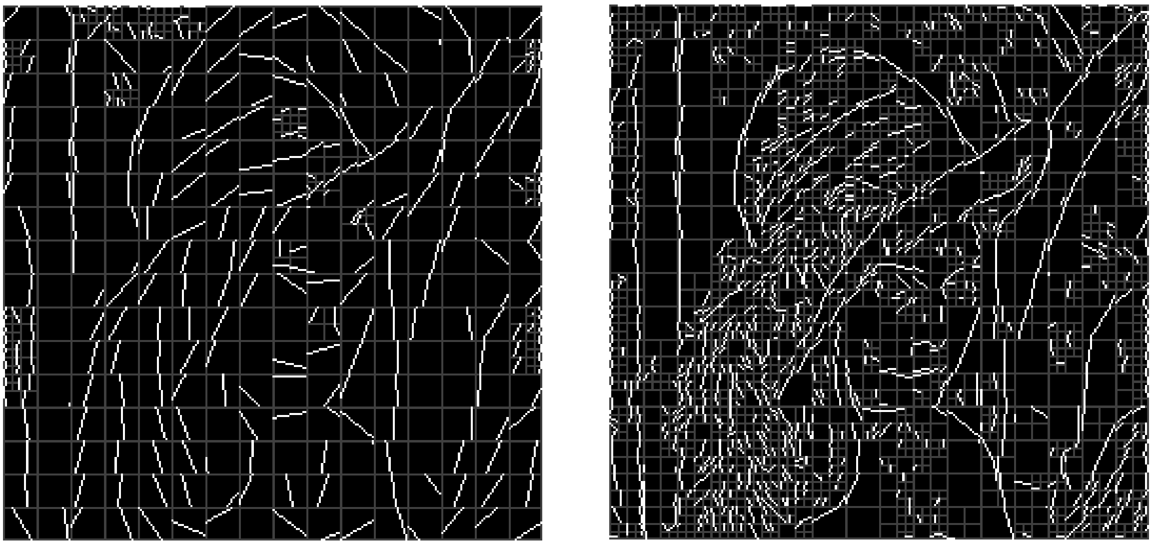

(a) $\alpha = 0.45, \gamma = 0.0$ (b) $\alpha = 0.45, \gamma = 0.7$

Figure 10: Segmentation results of Figure 9 with $\alpha = 0.45$ and different value of γ at level 4, 5 and 6

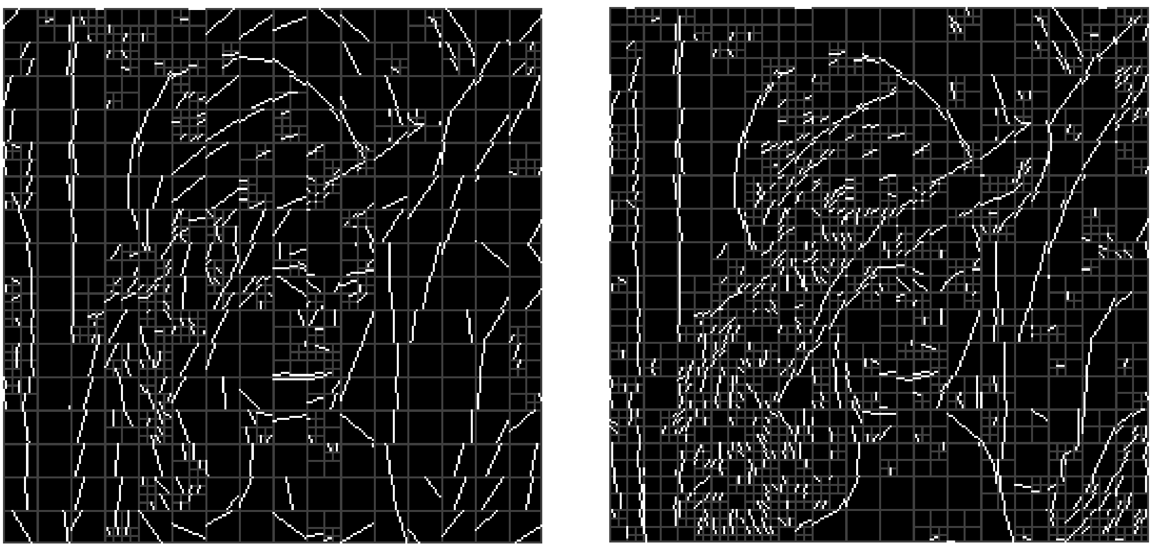

(a) $\alpha = 0.55, \gamma = 0.0$ (b) $\alpha = 0.55, \gamma = 0.7$

Figure 11: Segmentation results of Figure 9 with $\alpha = 0.55$ and different value of γ at level 4, 5 and 6

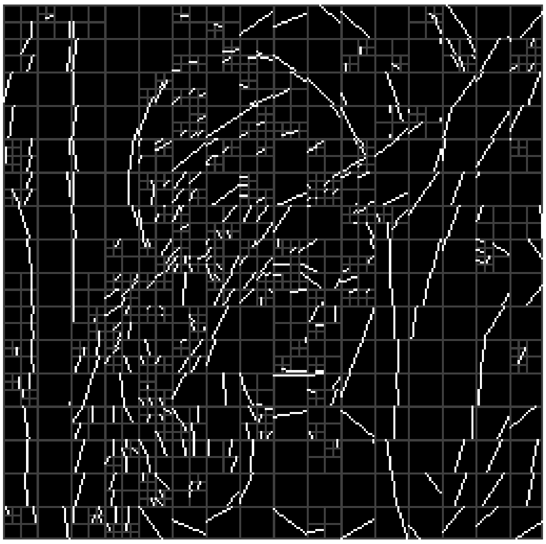

(a) $\alpha = 0.6, \gamma = 0.0$

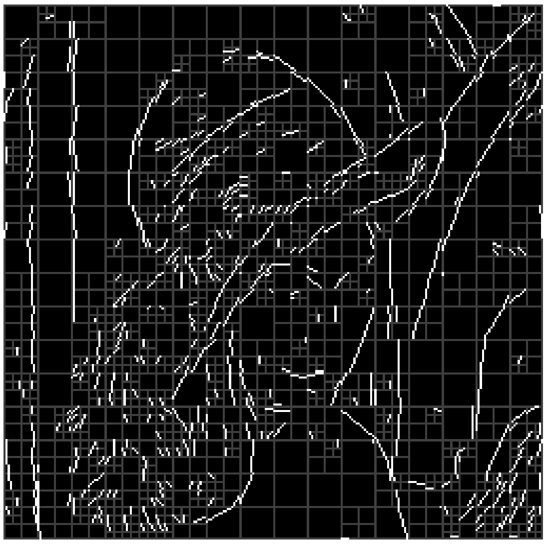

(b) $\alpha = 0.6, \gamma = 0.7$

Figure 12: Segmentation results of Figure 9 with $\alpha = 0.60$ and different value of γ at level 4, 5 and 6

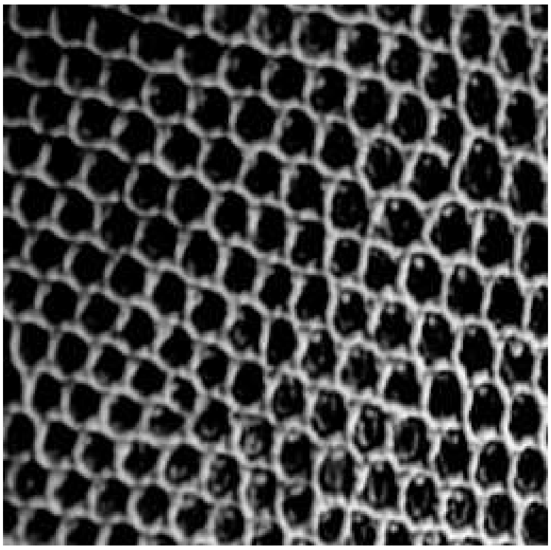

(a) Original image of reptile skin

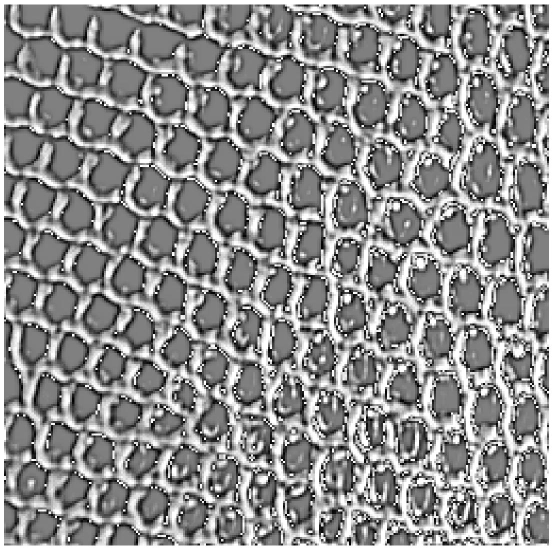

(b) high-pass filtered version of (a)

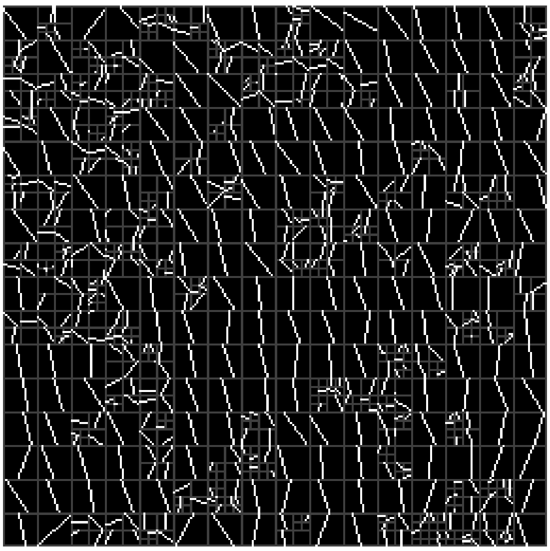

(c) features detected with $\alpha = 0.5$, $\gamma = 0.0$

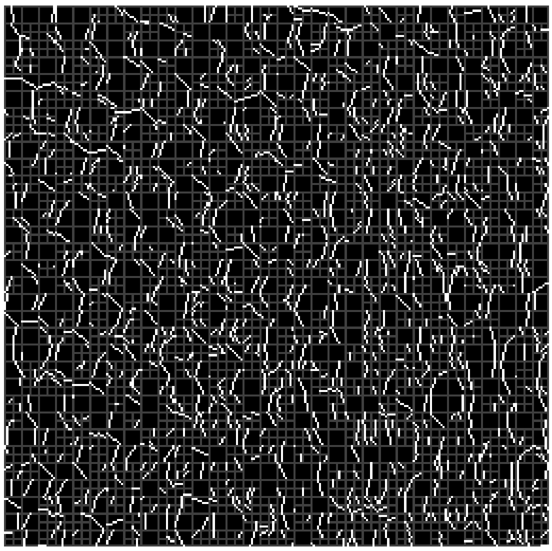

(d) features detected with $\alpha = 0.5$, $\gamma = 0.7$

Figure 13: Segmentation results of reptile skin at level 4, 5 and 6

References

[1] A. I. Borisenko and I. E. Tarapov. *Vector and Tensor Analysis with Applications*. Dover, 1979.

[2] P. J. Burt and E. H. Adelson. The Laplacian Pyramid as a Compact Image Code. *IEEE Transactions on Communication*, COM-31:532–540, 1983.

[3] A. Calway. *The Multiresolution Fourier Transform: A Genera Purpose Tool for Image Analysis*. PhD thesis, Department of Computer Science, The University of Warwick, UK, September 1989.

[4] Andrew R. Davies. *Image Feature Analysis using the Multiresolution Fourier Transform*. PhD thesis, Department of Computer Science, The University of Warwick, UK, 1993.

[5] Leif Haglund. *Adaptive Multidimensional Filtering*. PhD thesis, Department of Electrical Engineering, Linköping University, Sweden, 1992.

[6] R. Haralick. Statistical and structural approaches to texture. *IEEE*, 67(5):610–621, 1979.

[7] T. I. Hsu. *Texture Analysis and Synthesis using Multiresolution Fourier Transform*. PhD thesis, Department of Computer Science, The University of Warwick, UK, 1994.

[8] K. I. Laws. *Textured Image Segmentation*. PhD thesis, University of Southern California, USA, 1980.

[9] Peter Meulemans. Feature Extraction for Very Low Bit Rate Video Coding. Technical report, Department of Computer Science, University of Warwick, 1995.

[10] Athanasios Papoulis. *Signal Analysis*. McGraw Hill, 1981.

[11] A. Rosenfeld, R. A. Hummel, and S. W. Zucker. Scene Labelling by Relaxation Operations. 6:420–433, 1976.

[12] Michael Spann. *Texture Description and Segmentation in Image Processing*. PhD thesis, The University of Aston in Birmingham, UK, 1985.

[13] Carl-Fredrik Westin. *A Tensor Framework for Multidimensional Signal Processing*. PhD thesis, Department of Electrical Engineering, Linköping University, Sweden, 1994.

[14] R. Wilson, A. Calway, and E.R.S. Pearson. A Generalised Wavelet Transform for Fourier Analysis: The Multiresolution Fourier Transform and Its Application to Image and Audio Signal Analysis. *IEEE Tran. IT*, 38(2), March 1992.

[15] R. Wilson and Michael Spann. *Image Segmentation and Uncertainty.* Research Studies Press, 1988.